Meltwater Penetration Through Temperate Ice Layers in the Percolation Zone at DYE-2, Greenland Ice Sheet

Samira Samimi[1], Shawn J. Marshall[1,2] and Michael MacFerrin[3]

[1] Department of Geography, University of Calgary, Calgary, Alberta, Canada
[2] Environment and Climate Change Canada, Gatineau, Quebec, Canada
[3] Cooperative Institute for Research in Environmental Sciences, University of Colorado, USA

Corresponding author: Samira Samimi (samira.samimi@ucalgary.ca)

Key Points:

- Time-domain reflectometry probes give direct measurements of meltwater infiltration in firn at DYE-2 on the southwest Greenland Ice Sheet.
- We document meltwater penetration through ice layers up to 12 cm thick in temperate firn.
- The wetting front and melting front developed in tandem, indicating coupled hydrological and thermodynamic controls on meltwater infiltration depth.

Abstract

Meltwater retention in the firn layer of the Greenland Ice Sheet has the potential to buffer sea level rise due to ice sheet melt. The capacity of the firn layer to store meltwater is unclear, however, because refrozen ice layers can act as impermeable barriers to meltwater percolation, promoting runoff rather than retention. We present time-domain reflectometry and thermistor data which demonstrate that meltwater successfully penetrates ice layers up to 12 cm thick in the near-surface firn at DYE-2, Greenland. Our observations indicate that ice layers within polar firn can be permeable when summer warming and latent heat release from meltwater refreezing raise firn temperatures to the melting point. The extent and depth of refreezing, as determined by the coupled thermodynamic and hydrological evolution in the firn, are more important than the presence of ice layers in governing meltwater infiltration and retention at our study site.

Plain Language Summary

Meltwater that percolates below the surface of the Greenland Ice Sheet is difficult to track; some of it contributes to runoff, mass loss, and sea level rise, but some meltwater refreezes and is retained within the system. Greenland has a large firn area, where multi-year snow that has not yet transitioned to glacial ice has pore space that can retain meltwater. To improve understanding of hydrological and mass balance processes in polar firn, we excavated two firn pits in the Greenland Ice Sheet accumulation area in spring, 2016, and instrumented these pits with thermistors and time-domain reflectometry (TDR) sensors, connected to continuously-recording dataloggers. These sensors allowed us to directly track the coupled thermal and hydrological evolution in the firn through the summer melt season. We recorded nearly identical conditions at each site, with evidence of meltwater infiltration to a depth of between 1.8 m and 2.1 m and a wetting front that was thermally controlled, i.e. coincided with the melting front. This included meltwater penetration through numerous ice layers, including layers up to 12 cm thick. All of this meltwater refroze. Our results indicate that ice layers do not necessarily act as impermeable barriers to meltwater percolation and retention.

1 Introduction

Mass loss from the Greenland Ice Sheet has increased in recent decades due to significant increases in meltwater runoff (van den Broeke et al., 2009; Bamber et al., 2018; Mouginot et al., 2019). One of the challenges in estimating the current and future contribution of the ice sheet to sea level rise is the fact that surface melting does not always lead to runoff. In the percolation zone, meltwater that infiltrates the underlying cold snow or firn can be retained as liquid water (Forster et al., 2014; Koenig et al., 2014) or as refrozen ice (Pfeffer et al., 1991; Pfeffer and Humphrey, 1998; Harper et al., 2012). This reduces summer runoff and ice sheet contributions to sea level rise (Harper et al., 2012; Rennerhalm et al., 2013). Meltwater retention processes may be increasingly important as melting propagates to higher elevations in Greenland in a warming world (Vernon et al., 2013).

Meltwater that percolates and refreezes is difficult to account for in altimetric measurements of surface mass balance, as it is not possible to detect how much meltwater is retained within the system. This is also a source of uncertainty in mass balance models, as processes of meltwater percolation and refreezing occur at fine scales, are spatially heterogeneous, and *in situ* observations are scarce (*e.g.*, Harper et al., 2012; van As et al., 2016; Verjans et al., 2019, Vandecrux et al, 2019). This makes it difficult to calibrate and validate models of these processes, particularly on the scale of polar ice caps and ice sheets.

The extent to which meltwater retention in firn can buffer mass loss and sea-level rise is also unclear. Greenland's firn zone covers about 80% of the ice sheet, but refrozen near-surface ice layers have the potential to act as impermeable barriers, redirecting meltwater percolation into runoff (Gascon et al., 2013; Noel et al., 2017; MacFerrin et al., 2019; Ashmore et al., 2020). In the percolation zone, firn densification associated with warming and refreezing is also leading to a loss of available pore space, imposing further limits on meltwater storage capacity as melting progresses inland (Vandecrux et al., 2019). These processes can increase the ratio of meltwater runoff to retention. Hence, models of meltwater infiltration also need to account for ice-layer and firn-densification processes. These represent significant uncertainties in projections of the Greenland ice sheet's response to climate warming.

To examine meltwater infiltration and refreezing processes in the Greenland ice sheet percolation zone, we instrumented two firn pits with arrays of thermistors and time-domain reflectometry (TDR) sensors in order to track the coupled thermal and hydrological evolution in the seasonal snow and the upper ~3 m of firn through a summer melt season. The TDR sensors provide continuous measurements of dielectric permittivity, a proxy for liquid water content in the snow and firn. This manuscript presents these *in situ* observations and their implications for meltwater retention in firn. The experiment builds on Humphrey et al. (2012), who used thermistor arrays to track the thermal signature of meltwater infiltration in firn, which is apparent through the latent heat release when meltwater refreezes. Through the addition of TDR probes, we directly trace meltwater flow in the near-surface snow and firn. A similar experimental setup in the Canadian Rocky Mountains successfully demonstrated the ability to track meltwater percolation, refreezing, and snow-water content in a supraglacial snowpack using TDR probes (Samimi and Marshall, 2017). The implementation in Greenland extends these methods to polar firn, where liquid water content is lower and meltwater refreezing is more significant.

2 Methods

Measurements were established in May, 2016 in two firn pits near DYE-2 station in southwestern Greenland (see Figure S1 in the Supporting Information). The study sites, denoted A and B, were at an elevation of 2120 m, representing the upper percolation zone in southern Greenland (Harper et al., 2012). Co-ordinates of each firn pit are included in Table S1. During our 2016 field campaign, colleagues from Ludwig Maximilian University, Munich, also investigated meltwater percolation at site A, using upward-penetrating radar installed at a depth of ~4 m below the surface (Heilig et al., 2018). This provides a complementary dataset concerning the depth of meltwater penetration in summer 2016.

Firn pits were excavated to depths of 5.3 m at Site A and 2.2 m at Site B. The pits were located 400 m apart (Figure S1), with Site B included to provide a sample of the spatial variability of meltwater infiltration under similar climatic and snow/firn conditions. Measurements were also concentrated closer to the surface at Site B (Figure 1). Snow and firn density were measured at 10-cm intervals in the firn pits, using a 100-cm^3 box cutter. Density values at the depths of sensor installatons are reported in Table S1. The 2015-2016 seasonal snowpack had a depth of ~0.9 m and was free of ice layers. The underlying firn was made up of a mixture of ice layers and porous firn, with numerous ice layers in the form of discrete or continuous horizontal bands. Several ice layers were more than 10-cm thick. Figure 1 presents the ice-layer stratigraphy at each site, based on analysis of firn cores drilled about 3 m from each firn pit. The firn cores provide higher-quality stratigraphic records, permitting accurate characterization of ice layer thickness and extent. Firn exhibits considerable small-scale heterogeneity in the location and thickness of ice layers, so the firn core stratigraphy differs from that of the pits. However, the total ice content and the number and thickness of ice layers were similar in the fire cores and in the pits, including the presence of thick ice layers (>10 cm) in the upper 2 m of firn (e.g., Figure 1c). We therefore consider the ice-layer stratigraphy in Figure 1 to be representative.

A chainsaw was used to cut through the thick ice layers and below ~2 m depth, where the firn became too dense for a shovel. The north-facing vertical face of each firn pit was instrumented with 8 thermistors and 8 time-domain reflectometry (TDR) probes to monitor snow water content. TDR measures bulk dielectric permittivity, ε_b, an excellent proxy for liquid water content in snow and firn (Denoth, 1994; Techel and Pielmeier, 2011). The relative dielectric permittivity of air, ice, and water are ε_a=1, $\varepsilon_i \sim 3.2$, and $\varepsilon_w \sim 80$. Because liquid water has such a high value compared to air and ice, the dielectric permittivity of snow increases strongly with liquid water content. Dielectric permittivity also increases with snow density, but water content is the main control on variations in ε_b (Stein et al., 1997; Schneebeli et al., 1998).

Installation depths for the thermistors and TDRs are indicated in Figure 1 and Table S1. Sensors were installed in pairs at 8 different depths in each pit, with thermistor and TDR probes inserted about 15 cm apart at each depth. Sensors were inserted horizontally into undisturbed snow and firn, with the probes extending 0.3 m into the wall of the firn pit. Sensor spacing with depth was irregular in order to concentrate observations near the surface as well as immediately above and below thick ice layers, to test whether these acted as impermeable barriers to water flow. Pits were filled in with snow after the sensors were installed, several weeks in advance of the summer melt season. The thermistors and TDR probes were wired to Campbell Scientific CR1000 dataloggers and data were recorded every 30 minutes from May 11 to October 28, 2016.

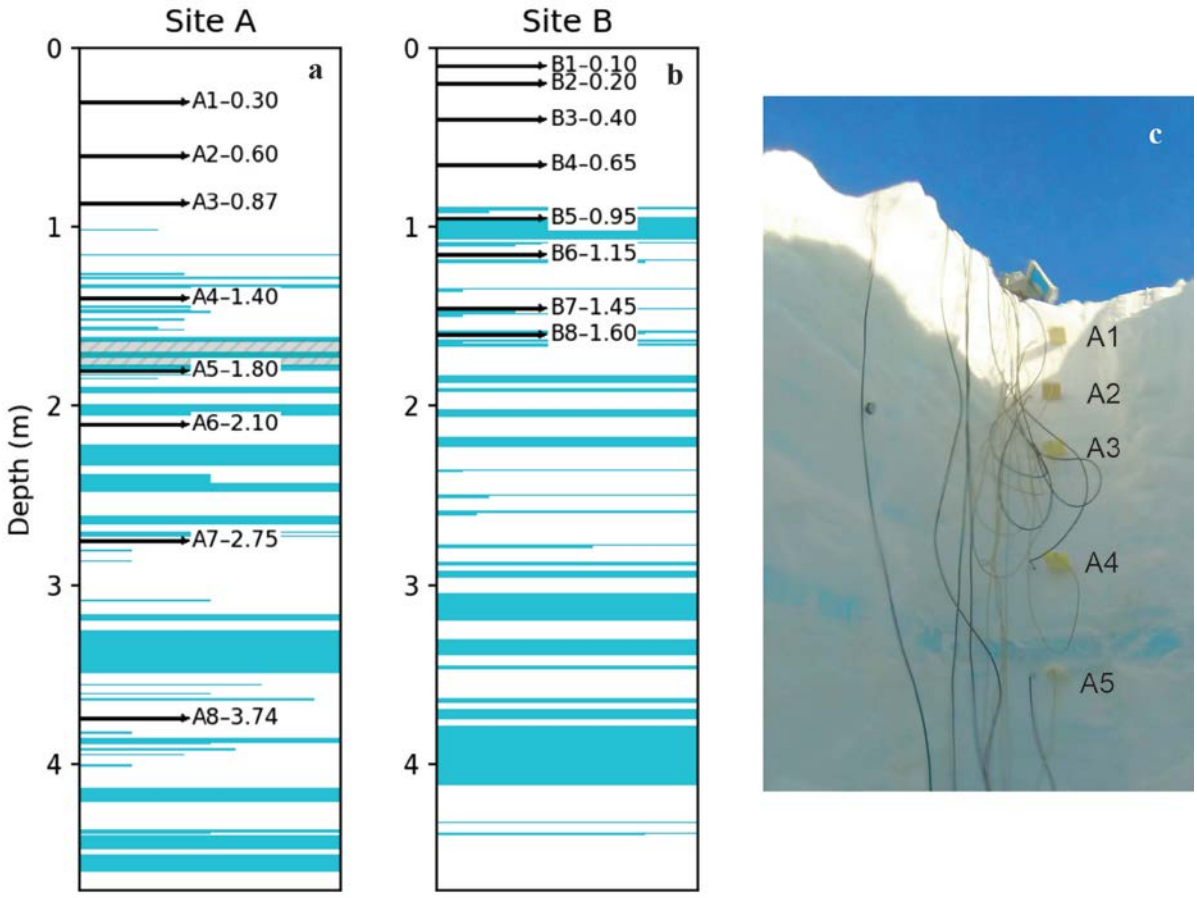

Figure 1. Ice-layer stratigraphy from sites a) A and b) B. Blue colors indicate ice layer location and thickness, and black arrows indicate the locations and depths (in m) of thermistors and TDR probes. The grey hatched zone in (a) highlights an 11-cm thick ice layer just above level A5 (1.68 to 1.79 m), as seen in photograph (c) of the upper ~2 m of pit A. The photograph also shows thermistor/TDR installations A1 to A5. Photograph by Samira Samimi.

We returned to the site in April 2017 to collect data and excavate the instruments. An automatic weather station (AWS) configured for surface energy balance monitoring was also installed adjacent to site A. Details on the AWS instrumentation and data processing are provided in the Supporting Information. All data were quality-controlled, and missing TDR data were gap-filled by linear interpolation. AWS data were used to calculate the surface energy fluxes and meltwater production over the summer, using the surface energy balance model of Ebrahimi and Marshall (2016) combined with a 1D subsurface model of the coupled thermal and hydrological evolution in the upper 10 m of snow and firn. The subsurface model considers thermal diffusion, advective heat transport from meltwater advection, and latent heat release from meltwater refreezing, combined with a simple model of meltwater percolation (Samimi and Marshall, 2017). The Supporting Information discusses the energy balance and subsurface models in detail.

3 Results and Analysis

The summer 2016 melt season ran from the second week of June until late August, with the main period of melt from July 18 to August 9. Details of the AWS data, the modeled surface melt and energy fluxes, and the complete subsurface TDR and thermistor datasets are presented in the Supporting Information (Figures S2 and S3).

Figure 2 presents the observed air temperature, melt rates, and subsurface temperature and dielectric permittivity during the period of melt onset in the upper 1.4 m of each firn pit. Melt is calculated from the surface energy balance in the upper snow layer (0.1 m), and can occur when air temperature is below 0°C if surface snow/firn is at the melting point and net energy is positive. Dielectric permittivities are plotted as anomalies relative to the initial (dry) values at each site. Monitoring depths are not identical at sites A and B, but their nearest analogues are plotted in Figure 2, and are within 0.1 m of each other. Site B offers more resolution of the near-surface snowpack, with sensors at 0.1 and 0.2 m. The thermistor records from 0.3, 0.6, 0.9 and 1.4 m (Figures 2c,d) indicate the close agreement in snow/firn thermal evolution at these two sites. Correlation coefficients for the two sites exceed 0.99 at these four depths.

Atmospheric warming in the first two weeks of June drove snowpack warming, with surface melting beginning on June 5 and temperate conditions first evident at site B from June 11-16. The upper 0.2 m of the snowpack warmed abruptly to 0°C (Figure 2d), accompanied by increases in dielectric permittivity of ~0.4 to 0.9 (Figure 2f). Diurnal temperature peaks slightly greater than 0°C for the upper two thermistors are likely due to absorption of solar radiation transmitted through the surface snow. At and below 0.3 m, the snowpack remained frozen and dry at both sites through this initial phase of melting. Snow at 0.3 m depth at site A came close to the melting point on June 14, reaching –0.3°C before cooling again (Figure 2c). Because the initial pulse of melting and refreezing was confined to the upper 0.2 m of the snowpack, the summer melt onset was not detected at site A.

A second melt event followed a week of cooler temperatures (Figure 2a) and was marked by an abrupt subsurface warming on June 23, with the upper 0.6 m of snow becoming temperate and wet at both sites. Over a six-hour period, temperatures at 0.3 and 0.6 m at site A increased by 3.5 and 5.4°C, respectively, both reaching 0°C (Figure 2c). Deeper thermistors also registered this abrupt warming (e.g., +5.5°C over 32 hours at 0.9 m), but firn below ~0.6 m depth remained frozen and dry. Temperate and wet conditions persisted in the upper 0.3 m until July 2, at which point another cooling cycle forced a return to cold, dry conditions at both sites. All of the meltwater within the system appears to have refrozen at this time.

The summer melt season resumed on July 19, with a sustained period of melting conditions and meltwater penetration to 1.4 m depth (Figure 3). This was characterized by a third abrupt warming event, registered by the top five thermistors at site A and all thermistors at site B (Figures 3c,d). Dielectric permittivities rose sharply at these depths, coincident with temperatures reaching 0°C (Figures 3e,f), although the increase in ε_b was less for the deeper sensors. The upper two sensors at site B experienced more meltwater than underlying sites in either pit, with $\Delta\varepsilon_b$ values of up to 2 (Figure 3f). The abrupt onset of temperate, wet conditions in the upper snow and firn was followed by a more gradual warming below this, recorded at the sensors from

1.8 to 3.7 m depth (Figures 3c and S2b). The wetting front and the 0°C isotherm reached 1.8 m depth by August 12, but firn below this remained frozen and dry.

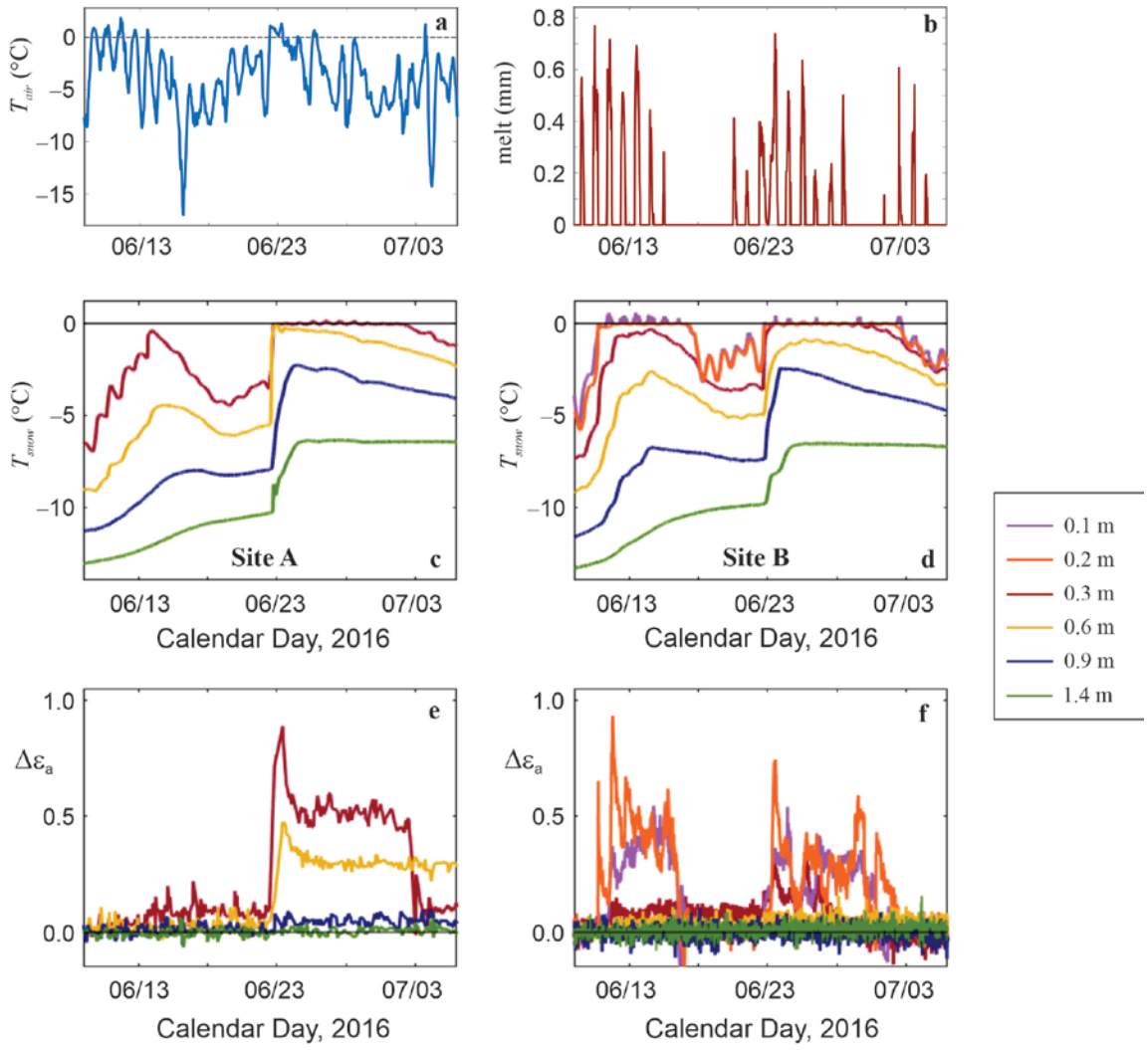

Figure 2. Observations during the onset of summer melt, June 9 to July 6, 2016: (a) air temperature, (b) modelled 30-minute melt (mm w.e.), (c,d) snow temperatures and (e,f) dielectric permittivity anomalies. Data in (c) to (f) are for the upper 1.4 m of firn pits A (left) and B (right). The legend applies to plots (c) to (f); values at 0.1 and 0.2 m were only measured at Site B.

Atmospheric cooling in mid-August (Figure 3a) caused the upper 0.3 m of the snowpack to refreeze ($\varepsilon_b \sim \varepsilon_{b0}$), but there was a temperate layer from about 0.6 m to 1.4 m, sandwiched between sub-zero conditions above and below (Figures 3c,d). This was most strongly evident at 0.9 m, where temperate, wet conditions persisted until August 22 at both sites. These middle layers of the firn pits were the last to refreeze, as latent heat of refreezing meltwater maintained temperate conditions at these depths for several days before seasonal cooling ensued.

There is no indication of meltwater percolation below the surface after August 22. Low rates of melting continued for several more days until shutting down for the summer on August 28, with an average melt rate of 2.9 mm w.e. d^{-1} from August 23-28. The upper snowpack warmed at both sites during these days, but ε_b remained at background levels. This is the only time over the summer when temperate snow conditions were not accompanied by evidence of liquid water. This melt event came following an atmospheric cooling cycle (Figure 3a) which caused the upper 0.3 m of the snowpack to refreeze and drop to temperatures of –2 to –5°C (Figure 3c,d). Combined with the low melt rates, the cold content of the snow appears to have been sufficient for meltwater to refreeze near the surface, above the upper TDR probes. Latent heat generated by the near-surface refreezing may have conductively warmed the underlying snow, but without meltwater infiltration.

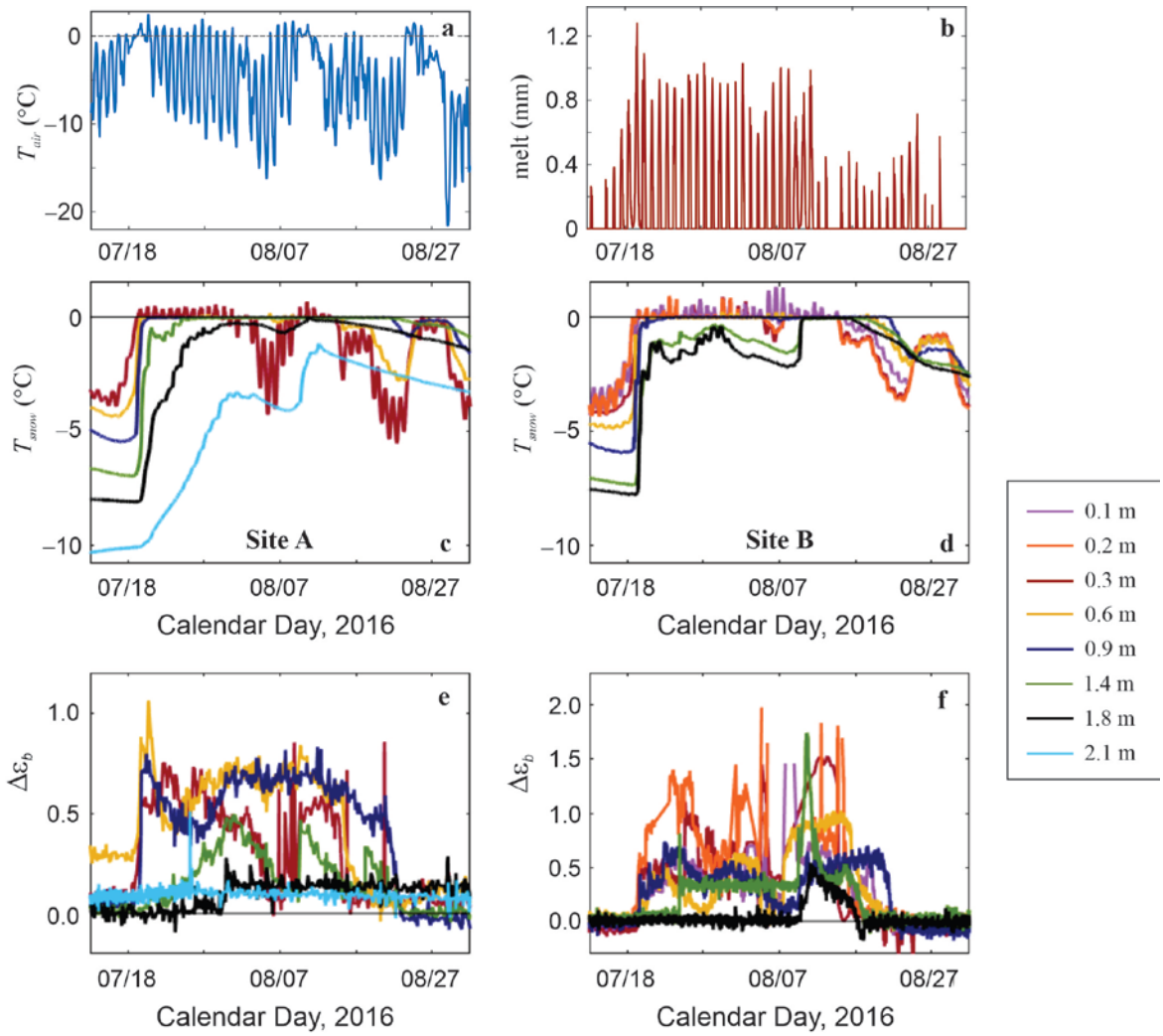

Figure 3. Same as Figure 2 but showing the main summer melt season from July 13 to September 1, 2016, and subsurface data in (c) to (f) are shown for the upper 2.1 m of the firn pits. Note the different scales in plots (e) and (f).

Overall, the evolution of subsurface temperatures and dielectric permittivities was similar at sites A and B, with evidence of thawing- and wetting-front propagation at the same times and to similar depths. Meltwater successfully penetrated several ice layers in the upper meter of firn at both sites. There were no ice layers in the winter snowpack, the upper ~0.9 m, but the underlying firn contained several discrete ice layers, some thin (1 mm to 2 cm), and others substantial. This included an 11-cm thick ice layer from 1.68 to 1.79 m depth at Site A and a 12-cm thick ice layer from 0.95 to 1.07 m depth at site B (Figure 1). In total over the upper 1.8 m, we measured 22 cm of ice in 11 discrete layers at site A and 19 cm of ice in 9 discrete layers at site B. Meltwater effectively penetrated through all of these ice layers, although not until temperatures reached the melting point at these depths.

4 Discussion

To our knowledge, these data represent the first continuous TDR measurements of meltwater infiltration in firn over a melt season. Combined with the thermistor records, the TDR data give a coherent account of the thermal evolution and meltwater infiltration at DYE-2 in summer 2016. The thawing front (0°C isotherm) and meltwater infiltration reached a depth of between 1.8 and 2.1 m. Below this, temperatures remained less than 0°C and dielectric permittivities did not rise above their background levels. This is in accord with observations from the upward-penetrating radar at site A, which also indicates penetration of the wetting front to about 2 m depth in summer 2016 (Heilig et al., 2018).

The data provide direct evidence of meltwater penetration through temperate ice layers in the Greenland percolation zone; ice layers did not act as impermeable barriers to meltwater infiltration. Rather, the depth of meltwater penetration at our sites was governed by the coupled hydrological and thermodynamic processes that determine the depth of the melting front (the 0°C isotherm). This in turn is a function of the net energy at the surface that is available to warm the snow and generate meltwater, the cold content, density, and structure (e.g., grain size) of the snow/firn (Colbeck, 1979; Colbeck and Anderson, 1982; Calonne et al., 2012), and the manner of meltwater infiltration, e.g., preferential flow processes (Humphrey et al., 2012; Hirashama et al., 2014; D'Amboise et al., 2017). The rate of melting is also important, through influences on near-surface saturation, refreezing capacity, and drainage processes.

The thawing/wetting front advanced to depth in step-wise fashion in our data. Four abrupt subsurface warming/wetting events were recorded over the summer, reaching progressively deeper into the snow and firn (Figures 2 and 3). These were seen simultaneously at the two sites and occurred during periods with positive air temperatures, but did not correspond to strong atmospheric warming events. Melt rates were high in these periods (Figures 2b and 3b), although not unusual. These events corresponded with increased or resumed surface melting following sustained cool (sub-zero) conditions. This indicates a potential role for restored cold content in the snow, which would increase refreezing capacity and latent heat release.

Subsurface warming occurs through a combination of latent heat release from meltwater refreezing, advective heat transfer associated with meltwater penetration into sub-zero snow, and thermal conduction, driven by heating of the surface layer in association with shortwave radiative fluxes and atmospheric warming. These mechanisms are clear in the thermistor data,

with gradual temperature shifts in response to atmospheric temperature fluctuations along with the abrupt subsurface warming events noted above. The sudden warming events are too rapid to be due to thermal conduction, so must be associated with meltwater advection and refreezing.

Modeled energy fluxes are described in detail in the Supplementary Material and illustrate the important role of latent heat flux in subsurface warming (Figure S4). Total summer latent heat release in the snow/firn is estimated to be 141 MJ m^{-2}, concentrated in the upper 0.3 m (Figure S4b). The model results give a good fit to the observational data and indicate that latent heat makes up 64.9% of the total summer (JJA) energy available to warm the subsurface snow and firn. Net energy at the surface during non-melt periods (i.e. sub-zero conditions) contributed an additional 76 MJ m^{-2} to warming the surface layer of the snowpack. This conductively warms the underlying snow and firn, accounting for 34.7% of the available subsurface energy. Positive net energy at the surface is particularly important in the early melt season (May and June), warming the snowpack prior to the onset of melt. After the onset of melt, meltwater infiltration drives deeper and more abrupt subsurface warming events, which are also captured in the model (Figure S4c). Meltwater advection made only a minor contribution to subsurface heat transport, estimated at 0.4% of the total energy available to warm the snow and firn.

Meltwater penetrated through multiple ice layers in the firn, permitting deeper meltwater infiltration and retention than would be possible if these layers acted as impermeable barriers. Two of the TDR sensors that experienced wetting were installed directly below thick, horizontally-continuous ice layers (sensors B6 and A5; see Figure 1c). While ice layers at our two sites were permeable, we can only speculate about the processes that permitted hydrological breakthrough. Fractures or discontinuities may have developed in the ice layers, or thawing to a temperate mixture of ice and water may have permitted water flux along interstitial grain boundaries and veins (e.g., Lliboutry, 1996). The effective permeability of ice layers and the relation to ice-layer thickness is an open question. There is evidence that thick ice layers in firn can be impermeable (Gascon et al., 2013; Ashmore et al., 2020), but meltwater infiltration through ice layers has also been observed or inferred (Humphrey et al., 2012; Machguth et al., 2016; Ashmore et al., 2020). Direct observations are needed to understand these processes and their efficacy with thicker ice layers, as found in the lower percolation zone of Greenland (Machguth et al., 2016; MacFerrin et al., 2019).

The similar evolution of the wetting front at our two sites, its progressive propagation to depth over the course of the melt season, the coherence with the upward-penetrating radar data near this site (Helig et al., 2018), and the ability to simulate the wetting front in a simple model of percolation flow (Figure S4) are all consistent with homogeneous infiltration of the wetting front. However, our measurements represent only two point locations, and the experimental design (vertically aligned sensors) does not permit conclusions concerning the mechanism(s) of meltwater infiltration. Preferential flow is thought to be the dominant process of meltwater infiltration in cold firn (e.g., Humphrey et al., 2012), and this may be what we recorded in summer 2016, if it proceeded in similar fashion at our two sites. Multiple instruments at each horizontal level would be needed to examine this.

Similarly, we cannot rule out meltwater penetration to depths greater than 2 m at other locations in the DYE-2 region in summer 2016. Spatial variability is a large challenge in understanding

and modeling firn hydrology and meltwater retention in Greenland. Our measurements nevertheless provide helpful insights to modelling efforts of meltwater infiltration into firn (*e.g.*, Wever et al., 2016; Steger et al., 2017), in particular the observation that ice layers can be permeable, permitting meltwater infiltration. Additional measurements like those reported here, especially during melt seasons of variable intensity, could help to track meltwater penetration into firn in the lower percolation zone and other sectors of Greenland.

Uncertainties

Sensor depths are reported as constant values in this manuscript, but actual depths changed over the course of the study, in association with fresh snowfall and surface ablation. Ultrasonic depth gauges were installed at each site to measure snow surface height (Figure S2d). All instruments at site A were deep enough to avoid melt-out. However, ablation from July 18 to August 9 was sufficient to expose the uppermost two sensors at site B (0.1 and 0.2 m), and inspection of the data is consistent with melt-out at these levels in the first week of August. A ~0.15 m snow event from August 10 to 12 buried the melted-out sensors and they give sensible signals again after this point, but data from August 5 to 12 are not reliable from these two levels.

There is a risk that water percolating in the disturbed area of the firn pits influences our sensors. although we see no evidence of this. The thermal and hydrological evolution are virtually identical at the two sites and are consistent with the upward-penetrating radar results of Helig et al. (2018), which measure the wetting front advance in undisturbed overlying firn. In addition, meltwater only penetrates to limited depths with each abrupt event; the pits were excavated to below the lower-most sensors, so free-flowing water in the disturbed areas would be expected to propagate deeper. Finally, the low rates of meltwater production and low-sloping environment at DYE-2 are more conducive to vertical infiltration than lateral flows. We are confident that the data reflect vertical meltwater infiltration from above, without influence from the adjacent pits, but this cannot be ruled out. Unfortunately, undisturbed control experiments are not feasible.

5 Conclusions

The thermistor, TDR, and AWS data provide a consistent and detailed account of the coupled thermodynamic and hydrological processes governing meltwater percolation and refreezing at DYE-2. This dataset presents an excellent opportunity to constrain the effective thermal and hydraulic conductivities of polar snow and firn, which will inform models of firn hydrology. Additional measurements are needed to test and confirm the inferred processes at other locations in Greenland's percolation zone.

Measurements from the two sites 400 m apart are exceptionally coherent, and indicate that meltwater at DYE-2 percolated to a depth of about 2 m in summer 2016. The wetting and melting fronts were coincident at the two sites, testifying to the coupled thermodynamic and hydrological controls on meltwater infiltration in firn. Meltwater penetrated through ice layers up to 12 cm thick. We are uncertain of the mechanical or thermodynamic processes that facilitate ice-layer permeability, but there is no evidence of meltwater infiltration through ice layers until temperatures reached 0°C. This requires sufficient latent heat release in the overlying firn and snow, which depends on the available pore space, cold content, and meltwater supply. Ice slabs

that are thick or close to the surface may be difficult to thaw, as heat transfer is reduced once firn is temperate or saturated. Models of this process can help to project whether meltwater is likely to infiltrate vertically or be redirected laterally, contributing to ice sheet runoff.

Acknowledgements

We thank Baptiste Vandecrux, Darren Hill, Achim Heilig, Liam Colgan, Bastian Gerling, and Leander Gambal for support with the field work. The U.S. National Science Foundation, Air National Guard, and CH2MHill Polar Field Services provided essential logistical support for this field work. Research costs of SS and SJM were supported by the Natural Sciences and Engineering Research Council (NSERC) of Canada, and funding for MM and the FirnCover project was from NASA Award NNX15AC62G. Data from this study are archived in the University of Calgary data repository, https://doi.org/10.5683/SP2/2QY39K. The authors declare no conflict of interest with the methods or results of this study.

References

Ashmore D. W, Mair D. W. F., and Burgess, D. O. (2020). Meltwater percolation, impermeable layer formation and runoff buffering on Devon Ice Cap, Canada. *Journal of Glaciology*, *66* (255), 61-73, https://doi.org/ 10.1017/jog.2019.80

Bamber, J. L., Westaway, R. M., Marzeion, B., & Wouters, B. (2018). The land ice contribution to sea level during the satellite era. *Environmental Research Letters*, *13* (6), 1–21.

Brock, B. W., Willis, I. C., & Sharp, M. J. (2006). Measurement and parameterisation of aerodynamic roughness length variations at Haut Glacier D'Arolla, Switzerland. *Journal of Glaciology*, *52* (177), 281–297

Calonne, N., Geindreau, C., Flin, F., Morin, S., Lesaffre, B., Rolland du Roscoat, S., & Charrier, P. (2012). 3-D image-based numerical computations of snow permeability: links to specific surface area, density, and microstructural anisotropy. *The Cryosphere*, *6*, 939–951, https://doi.org/10.5194/tc-6-939-2012.

Colbeck, S. C. (1979). Water flow through heterogeneous snow. *Cold Regions Science and Technol*ogy, *1*, 37–45, https://doi.org/10.1016/0165- 232X(79)90017-X.

Colbeck, S. C., & Anderson, E. A. (1982). The permeability of a melting snow cover. *Water Resources Research*, *18* (4), 904-908, https://doi.org/10.1029/WR018i004p00904.

Cuffey, K. M., & Paterson, W. S. B. (2010). *The Physics of Glaciers*, 4th Ed.

D'Amboise, C. J. L., Müller, K., Oxarango, L., Morin, S., and Schuler, T. V. (2017). Implementation of a physically based water percolation routine in the Crocus/SURFEX (V7.3) snowpack model. *Geoscience Model Development*, *10*, 3547–3566, https://doi.org/10.5194/gmd-10-3547-2017.

Denoth, A. (1994). An electronic device for long-term snow wetness recording. *Annals of Glaciology*, *19* (1), 104-106, https://doi.org/10.3189/S0260305500011058.

Ebrahimi, S., & Marshall, S. J. (2016). Surface energy balance sensitivity to meteorological variability on Haig Glacier, Canadian Rocky Mountains, *The Cryosphere*, *10*, 2799–2819, https://doi.org/10.5194/tc-10-2799-2016.

Forster, R. R., Box, J. E., van den Broeke, M. R., Miège, C., Burgess, E. W., Van Angelen, J. H., et al. (2014). Extensive liquid meltwater storage in firn within the Greenland ice sheet. *Nature Geoscience*, *7* (2), 95-98, https://doi.org/10.1038/ngeo2043.

Gascon, G., Sharp, M., Burgess, D., Bezeau, P., and Bush, A. B. G. (2013). Changes in accumulation-area firn stratigraphy and meltwater flow during a period of climate warming: Devon Ice Cap, Nunavut, Canada, *Journal of Geophysical Research, Earth Surfaces, 118*, 2380–2391, doi:10.1002/2013JF002838.

Harper, J., Humphrey, N., Pfeffer, W. T., Brown, J., & Fettweis, X. (2012). Greenland ice-sheet contribution to sea-level rise buffered by meltwater storage in firn. *Nature*, *491*, 240–243, doi: 10.1038/nature11566.

Heilig, A., Eisen, O., MacFerrin, M., Tedesco, M., & Fettweis, X. (2018). Seasonal monitoring of melt and accumulation within the deep percolation zone of the Greenland Ice Sheet and comparison with simulations of regional climate modeling. *Cryosphere*, *12*, 1851-1866. Doi: 10.5194/tc-12-1851-2018

Hirashima, H., Yamaguchi, S., & Katsushima, T. (2014). A multidimensional water transport model to reproduce preferential flow in the snowpack, *Cold Regions Science and Technology*, *108*, 80–90, https://doi.org/10.1016/j.coldregions.2014.09.004.

Humphrey, N. F., Harper, J. T., & Pfeffer, W. T. (2012). Thermal tracking of meltwater retention in Greenland's accumulation area. *Journal of Geophysical Research, 117*, F01010. https://doi.org/10.1029/2011JF002083.

Koenig, L. S., Miège, C., Forster, R. R., & Brucker, L. (2014). Initial in situ measurements of perennial meltwater storage in the Greenland firn aquifer. *Geophysical Research Letters, 41* (1), 81-85, https://doi.org/10.1002/2013GL058083.

Lliboutry, L. (1996). Temperate ice permeability, stability of water veins, and percolation of internal meltwater. *Journal of Glaciology*, *42* (141), 210-211.

MacFerrin, M., Machguth, H., van As, D., Charalampidis, C., Stevens, C. M., A. Heilig, A., et al. (2019). Rapid expansion of Greenland's low-permeability ice slabs. *Nature*, 573, 403-407, doi:10.1038/s41586-019-1550-3.

Marks, D., & Dozier, J. (1992). Climate and energy exchange at the snow surface in the Alpine region of the Sierra Nevada: 2. Snow cover energy balance. *Water Resources Research*, *28*, 3043–3054, https://doi.org/10.1029/92WR01483.

Mouginot, J., Rignot, E., Bjørk, A. A., van den Broeke, M., Millan, R., Morlighem, M., et al. (2019). Forty-six years of Greenland Ice Sheet mass balance from 1972 to 2018. *Proceedings of the U.S. National Academy of Sciences*, *116* (19), 9239-9244, https://doi.org/10.1073/pnas.1904242116.

Noël, B., van de Berg, W. J., Lhermitte, S., Wouters, B., Machguth, H., Howat, I., et al. (2017). A tipping point in refreezing accelerates mass loss of Greenland's glaciers and ice caps. *Nature Communications*, *8* (1), 1-8, doi:10.1038/ncomms14730.

Pfeffer, W. T., M. F. Meier, & Illangasekare, T. H. (1991). Retention of Greenland runoff by refreezing: Implications for projected future sea level change, *Journal of Geophysical Research*, *96* (C12), 22117–22124, doi:10.1029/91JC02502.

Pfeffer, W. T., & Humphrey, N. F. (1998). Formation of ice layers by infiltration and refreezing of meltwater. *Annals of Glaciology*, *26*, 83-91, https://doi.org/10.3189/*1998AoG26*-1-*83-91*.

Rennermalm, A. K., Moustafa, S. E., Mioduszewski, J., Chu, V. W., Forster, R. R., Hagedorn, B., et al. (2013). Understanding Greenland ice sheet hydrology using an integrated multi-

scale approach. *Environmental Research Letters*, *8* (1), 015017, doi: 10.1088/1748-9326/8/1/015017.

Samimi, S., & Marshall, S. J. (2017). Diurnal cycles of meltwater percolation, refreezing, and drainage in the supraglacial snowpack of Haig glacier, Canadian Rocky Mountains. *Frontiers in Earth Science*, *5*, 6, https://doi.org/10.3389/feart.2017.00006.

Schneebeli, M., Coléou, C., Touvier, F. & Lesaffre, B. (1998). Measurement of density and wetness in snow using time-domain reflectometry. *Annals of Glaciol*ogy, *26*, 69-72, https://doi.org/10.3189/*1998AoG26*-1-*69-72*.

Steger, C. R., Reijmer, C. H., van den Broeke, M. R., Wever, N., Forster, R. R., Koenig, L. S., et al. (2017). Firn meltwater retention on the Greenland Ice Sheet: a model comparison. *Frontiers in Earth Science*, *5* (3), https://doi.org/10.3389/feart.2017.00003.

Stein, J., Laberge, G., & Lévesque, D. (1997). Monitoring the dry density and the liquid water content of snow using time domain reflectometry (TDR). *Cold Regions Science and Technology*, *25* (2), 123-136, doi:10.1016/S0165-232X(96)00022-5.

Techel, F., & Pielmeier, C. (2011). Point observations of liquid water content in wet snow – investigating methodical, spatial and temporal aspects. *The Cryosphere*, *5*, 405-418, doi:10.5194/tc-5-405-2011.

van As, D., Box, J. E., & Fausto, R. S. (2016). Challenges of quantifying meltwater retention in snow and firn: an expert elicitation. *Frontiers in Earth Science*, *4* (101), https://doi.org/10.3389/feart.2016.00101.

van den Broeke, M., Bamber, J., Ettema, J., Rignot, E., Schrama, E., van de Berg, W. J., et al. (2009). Partitioning recent Greenland mass loss. *Science*, *326* (5955), 984-986, doi: 10.1126/science.1178176.

Vandecrux, B., MacFerrin, M., Machguth, H., Colgan, W. T., van As, D., Heilig, A., et al. (2019). Firn data compilation reveals widespread decrease of firn air content in western Greenland. *The Cryosphere*, 13, 845–859, https://doi.org/10.5194/tc-13-845-2019.

Verjans, V., Leeson, A. A., Stevens, C. M., MacFerrin, M., Noël, B., & van den Broeke, M. R. (2019). Development of physically-based liquid water schemes for Greenland firn-densification models. *The Cryosphere*, 13, 1819-1842, https://doi.org/10.5194/tc-13-1819-2019.

Vernon, C. L., Bamber, J. L., Box, J. E., van den Broeke, M. R., Fettweis, X., Hanna, E., & Huybrechts, P. (2013). Surface mass balance model intercomparison for the Greenland ice sheet. *The Cryosphere*, *7*, 599–614, https://doi.org/10.5194/tc-7-599-2013.

Wever, N., Würzer, S., Fierz, C., & Lehning, M. (2016). Simulating ice layer formation under the presence of preferential flow in layered snowpacks. *The Cryosphere*, *10*, 2731–2744, https://doi.org/10.5194/tc-10-2731-2016.